

RECEIVED: January 31, 2023

REVISED: March 12, 2023

ACCEPTED: April 11, 2023

PUBLISHED: May 9, 2023

Helicity amplitude analysis of $\chi_{cJ} \rightarrow \phi\phi$



The BESIII collaboration

E-mail: besiii-publications@ihep.ac.cn

ABSTRACT: Using (447.9 ± 2.3) million $\psi(3686)$ events collected with the BESIII detector, the decays of $\chi_{cJ} \rightarrow \phi\phi$ ($J = 0, 1, 2$) have been studied via the decay $\psi(3686) \rightarrow \gamma\chi_{cJ}$. The branching fractions of the decays $\chi_{cJ} \rightarrow \phi\phi$ ($J = 0, 1, 2$) are determined to be $(8.59 \pm 0.27 \pm 0.20) \times 10^{-4}$, $(4.26 \pm 0.13 \pm 0.15) \times 10^{-4}$, and $(12.67 \pm 0.28 \pm 0.33) \times 10^{-4}$, respectively, which are the most precise measurements to date. From a helicity amplitude analysis of the process $\psi(3686) \rightarrow \gamma\chi_{cJ}, \chi_{cJ} \rightarrow \phi\phi, \phi \rightarrow K^+K^-$, the polarization parameters of the $\chi_{cJ} \rightarrow \phi\phi$ decays are determined for the first time.

KEYWORDS: e^+e^- Experiments

ARXIV EPRINT: [2301.12922](https://arxiv.org/abs/2301.12922)

Contents

1	Introduction	1
2	Detector and Monte Carlo simulation	3
3	Event selection and background analysis	3
4	Amplitude analysis	5
4.1	Helicity system	5
4.2	Helicity amplitude	6
4.3	χ_{cJ} mass resolution	8
4.4	Fit method	9
4.5	Fit results	10
5	Systematic uncertainties	12
6	Conclusion and discussion	13
	The ANTARES collaboration	19

1 Introduction

Decays of the χ_{cJ} ($J = 0, 1, 2$) states provide critical information to test Quantum Chromodynamics (QCD). In the quark model, the χ_{cJ} states are identified as P -wave triple charmonium states with spin, parity and charge conjugation J^{++} ($J = 0, 1, 2$). At leading order, the hadronic decays of χ_{cJ} are described by annihilations of charm and anti-charm quarks into two gluons and subsequent production of light and/or strange quarks. Early theoretical calculations for exclusive decays of χ_{cJ} into light hadrons have yielded smaller branching fractions than experimental measurements [1–3].

For a charmonium state $\psi(\lambda)$ decaying into light hadrons $h_1(\lambda_1)$ and $h_2(\lambda_2)$, the asymptotic behavior of the branching fraction is evaluated in perturbative QCD (pQCD) calculations [4] as

$$\mathcal{B}[\psi(\lambda) \rightarrow h_1(\lambda_1)h_2(\lambda_2)] \sim \left(\frac{\Lambda_{\text{QCD}}^2}{m_c^2} \right)^{|\lambda_1 + \lambda_2| + 2}, \quad (1.1)$$

where λ, λ_1 , and λ_2 denote the helicities of the corresponding hadrons, $m_c \approx 1.5 \text{ GeV}$ is the charm quark mass, and Λ_{QCD} denotes the QCD scale parameter. If the light-quark mass is neglected, the vector-gluon coupling conserves quark helicity leading to the helicity selection rule (HSR) [5]: $\lambda_1 + \lambda_2 = 0$. If the helicity configuration does not satisfy this relation, the branching fraction will be suppressed.

Decay channel	$\chi_{c0} \rightarrow \phi\phi$		$\chi_{c2} \rightarrow \phi\phi$	
Parameter	x	ω_1	ω_2	ω_4
pQCD	0.293 ± 0.030	0.812 ± 0.018	1.647 ± 0.067	0.344 ± 0.020
3P_0	0.515 ± 0.029	1.399 ± 0.580	0.971 ± 0.275	0.406 ± 0.017
$D\bar{D}$ loop	0.359 ± 0.019	1.285 ± 0.017	5.110 ± 0.057	0.465 ± 0.002

Table 1. Numerical results of predictions from pQCD [6], 3P_0 [9] and $D\bar{D}$ loop models [10].

The $\chi_{cJ} \rightarrow \phi\phi$ decays clearly demonstrate that the decay mechanism of the χ_{cJ} particles is currently not well understood. Following pQCD calculations [6], the χ_{c1} decay rate should be strongly suppressed compared to χ_{c0} and χ_{c2} , due to HSR [4] and the requirement of identical particle symmetry [7]. However, BESIII reported similar branching fractions of $\chi_{cJ} \rightarrow \phi\phi$ decays for χ_{c0} , χ_{c1} , and χ_{c2} , namely $\mathcal{B}(\chi_{c0} \rightarrow \phi\phi) = (7.8 \pm 0.4 \pm 0.8) \times 10^{-4}$, $\mathcal{B}(\chi_{c1} \rightarrow \phi\phi) = (4.1 \pm 0.3 \pm 0.4) \times 10^{-4}$, and $\mathcal{B}(\chi_{c2} \rightarrow \phi\phi) = (10.7 \pm 0.4 \pm 1.1) \times 10^{-4}$ [8].

The quark-pair creation model (3P_0) [9] and charm-loop ($D\bar{D}$ loop) contributions [10–12] have been proposed to interpret the measured branching fractions with the model parameters obtained from data. In ref. [10], the analysis of the ϕ meson polarization is identified as a key measurement to probe hadronic-loop effects in the $\chi_{cJ} \rightarrow \phi\phi$ decays. Moreover, the ratios of the helicity amplitudes are found to be effective in the discrimination between the proposed models as these ratios are less sensitive to the parameters used in the evaluation of the model prediction. Table 1 summarizes the helicity-amplitude ratios predicted by the considered theoretical models, where the uncertainties are due to the uncertainties of parameters involved in the calculation. The variable x is defined as the ratio of transverse over the longitudinal polarized helicity amplitudes of the ϕ meson in $\chi_{c0} \rightarrow \phi\phi$: $x = |F_{1,1}^0/F_{0,0}^0|$ and the variables ω_i ($i = 1, 2, 4$) indicate the ratios of transverse over longitudinal polarized helicity amplitudes of the ϕ meson in $\chi_{c2} \rightarrow \phi\phi$: $\omega_1 = |F_{0,1}^2/F_{0,0}^2|$, $\omega_2 = |F_{1,-1}^2/F_{0,0}^2|$, $\omega_4 = |F_{1,1}^2/F_{0,0}^2|$, where $F_{\lambda_1, \lambda_2}^{J=0,2}$ are the helicity amplitudes. The $\chi_{c1} \rightarrow \phi\phi$ helicity amplitudes allow to test the validity of the identical particle symmetry: in this context the helicity-amplitude ratios $u_1 = |F_{1,0}^1/F_{0,1}^1|$ and $u_2 = |F_{1,1}^1/F_{1,0}^1|$ are expected to be 1 and 0, respectively [9].

In this analysis, the $\chi_{cJ} \rightarrow \phi\phi$ decays are studied to extract the polarization parameters from a data sample corresponding to 448.1 million $\psi(3686)$ events [13] collected in e^+e^- annihilation with the BESIII detector. The measurements of polarization parameters provide further information to understand χ_{cJ} decay mechanisms, and to test the quark-pair-creation model and charm-quark loop contributions to reveal the evasion of HSR [11] in the χ_{cJ} decays. Moreover, improved measurements of the $\chi_{cJ} \rightarrow \phi\phi$ branching fractions are reported.

2 Detector and Monte Carlo simulation

The BESIII detector [14] records symmetric e^+e^- collisions provided by the BEPCII storage ring [15], which operates in the center-of-mass (CM) energy range from 2.00 to 4.95 GeV, with a peak luminosity of $1 \times 10^{33} \text{ cm}^{-2}\text{s}^{-1}$ achieved at $\sqrt{s} = 3.77 \text{ GeV}$. The cylindrical core of the BESIII detector covers 93% of the full solid angle and consists of a helium-based multilayer drift chamber (MDC), a plastic scintillator time-of-flight system (TOF), and a CsI(Tl) electromagnetic calorimeter (EMC), which are all enclosed in a superconducting solenoidal magnet providing a 1.0 T [16] (0.9 T in 2012) magnetic field. The solenoid is supported by an octagonal flux-return yoke with resistive plate counter muon identification modules interleaved with steel. The charged-particle momentum resolution at 1 GeV/ c is 0.5%, and the dE/dx resolution is 6% for electrons from Bhabha scattering. The EMC measures photon energies with a resolution of 2.5% (5%) at 1 GeV in the barrel (end cap) region. The time resolution in the TOF barrel region is 68 ps, while that in the end cap region is 110 ps.

Simulated data samples produced with a GEANT4-based [17] Monte Carlo (MC) package, which includes the geometric description of the BESIII detector and the detector response, are used to determine detection efficiencies and to estimate backgrounds. The simulation models the beam energy spread and initial state radiation (ISR) in the e^+e^- annihilations with the generator KKMC [18, 19]. Signal MC events for $\chi_{cJ}(J = 0, 1, 2) \rightarrow \phi\phi$ are generated by using the amplitude model with helicity amplitude ratios fixed to the results of this amplitude analysis. An inclusive MC sample, which includes the production of the 506 million $\psi(3686)$ resonance, the ISR production of the J/ψ , and the continuum processes incorporated in KKMC, is used for studying background contributions. All particle decays are modelled with EVTGEN [20, 21] using branching fractions either taken from the Particle Data Group [22], when available, or otherwise estimated with LUNDCHARM [23, 24]. Final state radiation (FSR) from charged final state particles is incorporated using the PHOTOS package [25].

3 Event selection and background analysis

The $\chi_{cJ} \rightarrow \phi\phi$ candidates are selected from the process $e^+e^- \rightarrow \psi(3686) \rightarrow \gamma\chi_{cJ}$. The $\gamma K^+K^-K^+K^-$ final state is selected by requiring four charged tracks with zero net charge and at least one photon shower. Charged tracks detected in the MDC are required to be within a polar angle (θ) range of $|\cos\theta| < 0.93$, where θ is defined with respect to the z -axis, which is the symmetry axis of the MDC. For charged tracks not originating from K_S^0 or Λ decays, the distance of closest approach to the interaction point (IP) must be less than 10 cm along the z -axis, $|V_z|$, and less than 1 cm in the transverse plane, $|V_{xy}|$. Photon candidates are identified using showers in the EMC. The deposited energy of each shower must be more than 25 MeV in the barrel region ($|\cos\theta| < 0.80$) and more than 50 MeV in the end cap region ($0.86 < |\cos\theta| < 0.92$). To exclude showers that originate from charged tracks, the angle subtended by the EMC shower and the position of the closest charged track at the EMC must be greater than 10 degrees as measured from the IP. To suppress

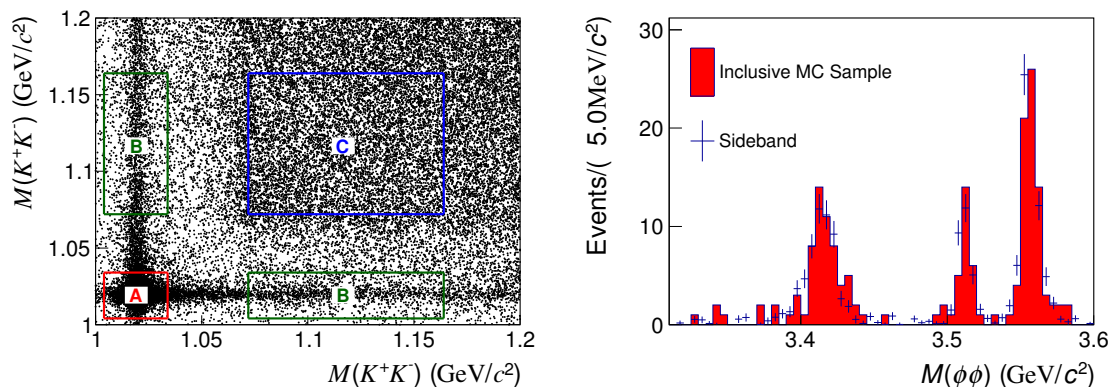


Figure 1. Left: distribution of $M(K^+K^-)$ versus $M(K^+K^-)$, two pairs of K^+K^- are plotted symmetrically; right: χ_{cJ} peaking backgrounds ($\chi_{cJ} \rightarrow \phi K^+K^-$ and $K^+K^-K^+K^-$) estimated from inclusive MC events and the sideband events in data.

electronic noise and showers unrelated to the event, the difference between the EMC time and the event start time is required to be within $[0,700]$ ns.

To improve the momentum resolution and to reduce the background contributions, the four charged tracks that are assumed to be kaons and one photon candidate are subjected to a kinematic fit constrained by four-momentum conservation (4C), with the hypothesis of the candidate events coming from $\psi(3686) \rightarrow \gamma 2(K^+K^-)$. Among all the photon candidates reconstructed in the event, only that providing the least χ_{4C}^2 value in the kinematic fit (χ_{4C}^2) is retained. Signal candidates are selected by requiring $\chi_{4C}^2 < 60$, which is optimized by the figure of merit $\frac{S}{\sqrt{S+B}}$, where S and B are the normalized numbers of signal and background events obtained from signal and inclusive MC sample, respectively. The intermediate ϕ mesons are reconstructed as the K^+K^- combinations that minimize the discriminator $\delta = \sqrt{(M_{K^+K^-}^{(1)} - m_\phi)^2 + (M_{K^+K^-}^{(2)} - m_\phi)^2}$, where $M_{K^+K^-}^{(i)}$ is the invariant mass of the K^+K^- combination i and m_ϕ is the known ϕ mass [22]. The ϕ signal region is defined as $|M_{K^+K^-} - m_\phi| < 0.015 \text{ GeV}/c^2$ from the study of simulated events, as shown in the area A in figure 1. This mass window is also applied for signal MC samples to obtain efficiency. Background events are subtracted using two sideband regions of data events corresponding to $\chi_{cJ} \rightarrow \phi K^+K^-$ and $K^+K^-K^+K^-$ in the following amplitude analysis. The ϕK^+K^- sideband region requires one pair of kaons to satisfy $|M_{K^+K^-}^{(1)} - m_\phi - 0.1 \text{ GeV}/c^2| < 3 \times 0.015 \text{ GeV}/c^2$ and the other pair to satisfy $|M_{K^+K^-}^{(2)} - m_\phi| < 0.015 \text{ GeV}/c^2$, illustrated as the area B in figure 1. The $K^+K^-K^+K^-$ sideband region requires both pairs of kaons to satisfy $|M_{K^+K^-}^{(1,2)} - m_\phi - 0.1 \text{ GeV}/c^2| < 3 \times 0.015 \text{ GeV}/c^2$, illustrated as the area C in figure 1.

By analyzing an inclusive MC sample corresponding to 506 million $\psi(3686)$ events, the number of background events is estimated to be 153 after applying the same reconstruction and selection procedure as for real data, which is about 1.7% in total MC events. The decay with the same final state, $\chi_{cJ} \rightarrow K^+K^-K^+K^-$ without intermediate states, is found to be the dominant background according the analysis of the event type of inclusive MC [26]. The shape and amount of the background events in the signal region are estimated

using the events in the sideband regions B and C . The scale factor for the events in each sideband region is determined through exclusive simulations of χ_{cJ} decays into $\phi K^+ K^-$ and $K^+ K^- K^+ K^-$. To be more specific, the number of selected sideband events is determined by the ratio of the number of events in the sideband region to the number of events in the signal region with an MC simulation for the $\phi K^+ K^-$ and $K^+ K^- K^+ K^-$ decays. The background contributions evaluated with the inclusive MC sample and with the sideband events in data are in good agreement as shown in the right of figure 1.

The background contribution from the continuum process $e^+ e^- \rightarrow 2(K^+ K^-) \gamma$ is studied with a data sample of $e^+ e^-$ annihilations collected at a center-of-mass (CM) system energy of 3.65 GeV, just below the $\psi(3686)$ resonance, and with an integrated luminosity of 42.6 pb^{-1} . The signal selection previously described, with the kinematic fit constraint adapted to the different CM system, does not show any event in the χ_{cJ} signal region. The contribution of the continuum process is therefore negligible.

4 Amplitude analysis

4.1 Helicity system

The selected $\chi_{cJ} \rightarrow \phi\phi$ events are subject of a helicity amplitude analysis to determine the polarization parameters. In the amplitude analysis, the joint angular distribution for the sequential decays $e^+ e^- \rightarrow \psi(3686) \rightarrow \gamma \chi_{cJ}$, $\chi_{cJ} \rightarrow \phi\phi$ and $\phi \rightarrow K^+ K^-$ is constructed in the helicity system of various intermediate resonances in the process, as shown in figure 2. The helicity axis for a particular decay is characterized by the momentum direction of the decaying particle in its mother particle rest frame. Starting from the unpolarized $e^+ e^-$ initial system, the helicity axes are defined as described below.

- For $e^+ e^- \rightarrow \psi(3686) \rightarrow \gamma \chi_{cJ}$, the polar angle θ_0 is defined as the angle spanned between the χ_{cJ} moving direction and the e^+ beam direction, which corresponds to the polar angle of the χ_{cJ} momentum in the $e^+ e^-$ CM system. The corresponding azimuthal angle follows figure 2 and cancels out in the amplitude of this decay.
- For $\chi_{cJ} \rightarrow \phi\phi$, the momenta of the two ϕ mesons define the χ_{cJ} decay plane. Due to momentum conservation, the momenta of the χ_{cJ} meson and the two ϕ mesons have to be located in the same decay plane. After boosting the two ϕ momenta to the χ_{cJ} rest frame, they are still in the same decay plane. Then the polar angle θ_1 is defined as the angle between the χ_{cJ} momentum and the ϕ momentum in the χ_{cJ} rest frame. The azimuthal angle ϕ_1 is defined as the angle between the χ_{cJ} production and decay planes.
- For each of the two $\phi \rightarrow K^+ K^-$ decays, the polar angle $\theta_2(\theta_3)$ is defined as the angle between the $K^+(K^-)$ momentum in the ϕ rest frame and the ϕ momentum in the χ_{cJ} rest frame. The corresponding angles ϕ_2 and ϕ_3 are defined as the angle spanned between the ϕ production and decay planes.

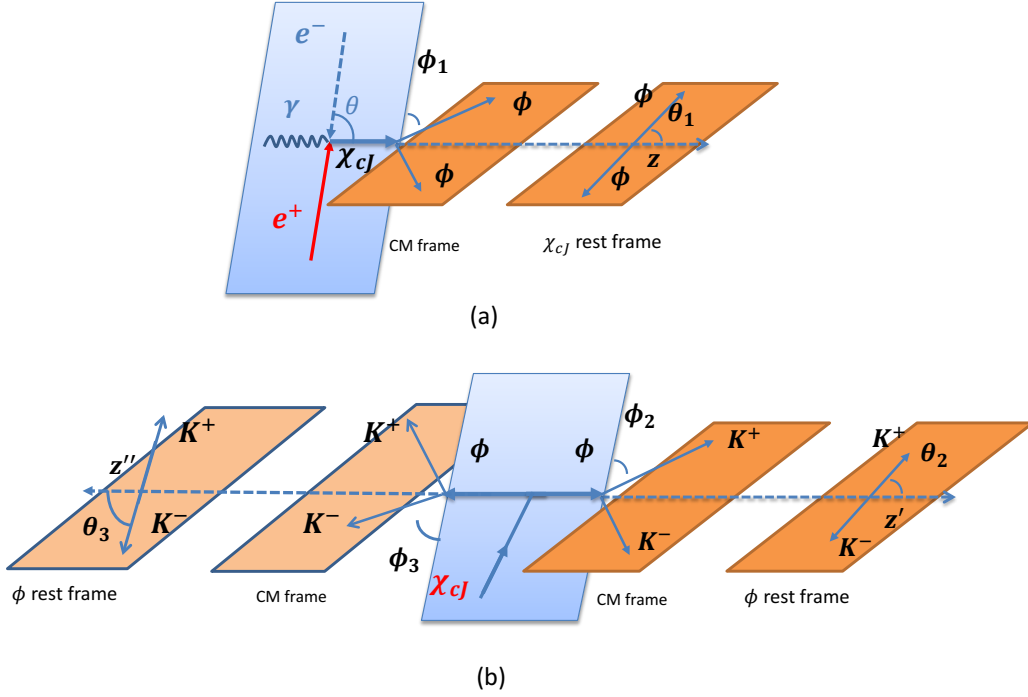


Figure 2. Definitions of helicity angles.

4.2 Helicity amplitude

Let X be a resonance of spin-parity J^η (with z -component M) and mass μ which decays into two particles 1 and 2, $X \rightarrow 1 + 2$, where the particle i has spin S_i , intrinsic parity η_i , and helicity λ_i (with $i = 1, 2$). In the rest frame of the resonance X , \vec{p} represents the momentum of the particle 1 with the spherical angles given by $\Omega = (\theta, \phi)$. \mathcal{M} is the decay operator. Then the helicity amplitude A for the two-body decay $X \rightarrow 1 + 2$ can be written as [27–29]

$$\begin{aligned} A &= \langle \vec{p}\lambda_1; -\vec{p}\lambda_2 | \mathcal{M} | JM \rangle \\ &= 4\pi \left(\frac{\mu}{p} \right)^{\frac{1}{2}} \langle \phi\theta\lambda_1\lambda_2 | JM\lambda_1\lambda_2 \rangle \langle JM\lambda_1\lambda_2 | \mathcal{M} | JM \rangle \\ &= N_J F_{\lambda_1, \lambda_2}^J D_{M, \lambda}^{J*}(\phi, \theta, 0), \lambda = \lambda_1 - \lambda_2, \end{aligned}$$

where $N_J = 4\pi \left(\frac{\mu}{p} \right)^{\frac{1}{2}}$ is a normalization factor and $D_{M, \lambda}^{J*}(\phi, \theta, 0)$ is the D -function [30]. Generally, the helicity amplitudes $F_{\lambda_1, \lambda_2}^J$ depend on the momenta of the final state particles. It can be expanded in terms of the L - S coupling scheme [27, 31]:

$$F_{\lambda_1, \lambda_2} = \sum_{LS} g_{LS} \sqrt{\frac{2L+1}{2J+1}} \langle L0S\lambda | J\lambda \rangle \langle S_1\lambda_1 S_2 - \lambda_2 | S\lambda \rangle r^L B_L(r) / B_L(r_0), \quad (4.1)$$

where g_{LS} is the coupling constant in the L - S coupling scheme; $\langle L0S\lambda | J\lambda \rangle$ and $\langle S_1\lambda_1 S_2 - \lambda_2 | S\lambda \rangle$ denote the Clebsch-Gordan coefficients; r is the momentum of the two final state particles, measured in the resonance rest frame, and r_0 is the corresponding quantity

Decay Mode	Helicity Angle	Amplitude
$\psi(3686)(M) \rightarrow R_i(\lambda_R) \gamma(\lambda_\gamma)$	θ_0	$A_{\lambda_\gamma, \lambda_R}^1 D_{M, \lambda_R - \lambda_\gamma}^{1*}(0, \theta_0, 0)$
$R_i(\lambda_R) \rightarrow \phi(\lambda_1)\phi(\lambda_2)$	θ_1, ϕ_1	$F_{\lambda_1, \lambda_2}^J D_{\lambda_R, \lambda_1 - \lambda_2}^{J*}(\phi_1, \theta_0, 0)$
$\phi(\lambda_1) \rightarrow K^+(0^-) K^-(0^-)$	θ_2, ϕ_2	$B_{0,0}^1 D_{\lambda_1, 0}^{1*}(\phi_2, \theta_2, 0)$
$\phi(\lambda_2) \rightarrow K^+(0^-) K^-(0^-)$	θ_3, ϕ_3	$B_{0,0}^1 D_{\lambda_2, 0}^{1*}(\phi_3, \theta_3, 0)$

Table 2. Definitions of helicity angles and amplitudes of sequential decays.

evaluated at the nominal mass of the resonance; B_L is a barrier factor, which depends on the angular momenta L reaching from 0 up to 4 and can be written as [32]

$$\begin{aligned}
 B_0(r)/B_0(r_0) &= 1, \\
 B_1(r)/B_1(r_0) &= \frac{\sqrt{1 + (dr_0)^2}}{\sqrt{1 + (dr)^2}}, \\
 B_2(r)/B_2(r_0) &= \frac{\sqrt{9 + 3(dr_0)^2 + (dr_0)^4}}{\sqrt{9 + 3(dr)^2 + (dr)^4}}, \\
 B_3(r)/B_3(r_0) &= \frac{\sqrt{225 + 45(dr_0)^2 + 6(dr_0)^4 + (dr_0)^6}}{\sqrt{225 + 45(dr)^2 + 6(dr)^4 + (dr)^6}}, \\
 B_4(r)/B_4(r_0) &= \frac{\sqrt{11025 + 1575(dr_0)^2 + 135(dr_0)^4 + 10(dr_0)^6 + (dr_0)^8}}{\sqrt{11025 + 1575(dr)^2 + 135(dr)^4 + 10(dr)^6 + (dr)^8}},
 \end{aligned} \tag{4.2}$$

where $d = 3 \text{ GeV}^{-1}$ is a constant [33].

Table 2 shows the definitions of helicity angles and amplitudes for the sequential process $\psi(3686) \rightarrow \gamma R_i$, $R_i \rightarrow \phi\phi$, and $\phi \rightarrow K^+K^-$.

Then the joint amplitude for the sequential process is obtained by

$$\begin{aligned}
 \mathcal{M}(R_i) &= \frac{1}{2} \sum_{M, \lambda_R, \lambda_1, \lambda_2} A_{\lambda_R, \lambda_\gamma}^1 D_{M, \lambda_R - \lambda_\gamma}^{1*}(0, \theta_0, 0) F_{\lambda_1, \lambda_2}^J D_{\lambda_R, \lambda_1 - \lambda_2}^{J*}(\phi_1, \theta_0, 0) \\
 &\quad \times B_{0,0}^1 D_{\lambda_1, 0}^{1*}(\phi_2, \theta_2, 0) B_{0,0}^1 D_{\lambda_2, 0}^{1*}(\phi_3, \theta_3, 0) BW(m_{\phi\phi}, m_i, \Gamma_i),
 \end{aligned} \tag{4.3}$$

with

$$BW(m_{\phi\phi}, m_i, \Gamma_i) = \frac{1}{m_{\phi\phi}^2 - m_i^2 + im_i\Gamma_i}, \tag{4.4}$$

where R_i can assume a resonant χ_{cJ} or a non-resonant (NR) contribution; M is the z -projection of the $\psi(3686)$ spin with $M = \pm 1$ since it is produced from unpolarized e^+e^- beams; $A_{\lambda_R, \lambda_\gamma}$, $F_{\lambda_1, \lambda_2}^J$, and $B_{0,0}^1$ are helicity amplitudes which are expanded in terms of the L - S coupling constant g_{LS} according to eq. (4.1), $m_{\phi\phi}$ is the invariant mass of the ϕ meson pair, m_i and Γ_i are mass and width of the corresponding χ_{cJ} , and $BW(m_{\phi\phi}, m_i, \Gamma_i)$ is a Breit-Wigner (BW) function for χ_{cJ} . In a consistent description of the non-resonant contribution, NR $\rightarrow \phi\phi$, in which the $\phi\phi$ system has quantum numbers $J^P = 0^\pm, 1^+$ and 2^+ , the BW function is set to 1. The BW functions for the two ϕ mesons are isolated from the above equation. They are taken into account in the MC event generation and used to estimate the normalization factor for the likelihood function. The ϕ BW function

Decay	Partial waves (LS)
$\psi(3686) \rightarrow \gamma\chi_{c0}$	(01), (21)
$\psi(3686) \rightarrow \gamma\chi_{c1}$	(01), (21), (22)
$\psi(3686) \rightarrow \gamma\chi_{c2}$	(01), (21), (22), (23), (43)
χ_{c0} or NR(0^+) $\rightarrow \phi\phi$	(00), (22)
χ_{c1} or NR(1^+) $\rightarrow \phi\phi$	(01), (21), (22)
χ_{c2} or NR(2^+) $\rightarrow \phi\phi$	(02), (20), (21), (22), (42)
NR(0^-) $\rightarrow \phi\phi$	(11)
$\phi \rightarrow K^+K^-$	(10)

Table 3. Involved partial waves (LS) in the joint angular distribution.

and the mass resolution are well simulated in the phase-space MC events of the decay $\psi(3686) \rightarrow \gamma\phi\phi \rightarrow \gamma 2K^+K^-$. It is noteworthy that this partial wave expansion ensures parity conservation of the helicity amplitude in the sequential decays. The allowed values for L and S of the corresponding subprocesses are given in table 3. The g_{LS} parameters involved in the fit are taken as complex numbers, and their values are determined from the fit to data.

The partial decay rate of $\psi(3686)$ is given by

$$d\sigma \propto \frac{1}{2} \sum_{M,\lambda_\gamma} \left| \sum_{R_i} \mathcal{M}(R_i) \right|^2 d\Phi, \quad (4.5)$$

where $d\Phi$ is the standard phase space for the decay $\psi(3686) \rightarrow \gamma\phi\phi$ with $\phi \rightarrow K^+K^-$. The summation is taken over $M = \pm 1$ due to the fact that the $\psi(3686)$ is produced from unpolarized e^+e^- beams.

4.3 χ_{cJ} mass resolution

The widths of the χ_{c0} , χ_{c1} , and χ_{c2} states are $\Gamma = 10.8 \pm 0.6, 0.84 \pm 0.04$, and 1.97 ± 0.09 MeV [22], respectively. Meanwhile, the mass resolution, whose magnitude is 4.6 MeV, is greater than χ_{c1} and χ_{c2} widths and therefore crucial in this analysis. The observed resonances can be well approximated using χ_{cJ} lineshapes convolved with the mass resolution function. Therefore, in the amplitude analysis, the BW function for the χ_{cJ} in eq. (4.3) is replaced with

$$|BW(m_{\phi\phi}, m_0, \Gamma)|^2 \rightarrow \int_{-\infty}^{+\infty} |BW(m'_{\phi\phi}, m_0, \Gamma)|^2 R(m'_{\phi\phi} - m_{\phi\phi}) dm'_{\phi\phi}, \quad (4.6)$$

where $R(m)$ is the mass resolution function, which is determined from MC simulations. The detector resolution function is parametrized with a three-Gaussian function, i.e.

$$R(m_{\phi\phi}) = f_1 |G(m_{\phi\phi}, m_1, \sigma_1)|^2 + f_2 |G(m_{\phi\phi}, m_2, \sigma_2)|^2 + (1 - f_1 - f_2) |G(m_{\phi\phi}, m_3, \sigma_3)|^2, \quad (4.7)$$

where m_j and σ_j are the mean and width of the j -th Gaussian function (G), $j = 1, 2, 3$. For each χ_{cJ} state, the fraction parameters f_1 and f_2 are determined by fitting the χ_{cJ} lineshape.

4.4 Fit method

The relative magnitudes and phases of the coupling constants, g_{LS} , are determined by an unbinned maximum likelihood fit. The joint likelihood for observing N events in the data set is

$$\mathcal{L} = \prod_{i=1}^N P(x_i), \quad (4.8)$$

where $P(x_i)$ is the probability to produce event i with a set of four-momenta x_i . The normalized $P(x_i)$ is calculated from the differential cross section

$$P(x_i) = \frac{(d\sigma/d\Phi)_i}{\sigma_{\text{MC}}}, \quad (4.9)$$

where σ_{MC} is calculated using a set of MC events. MC events are generated according to a phase space distribution and are subject to the detector simulation. Simulated events pass the same reconstruction and selection criteria as events recorded by the detector. For an MC sample with sufficient statistics, σ_{MC} is evaluated with

$$\sigma_{\text{MC}} = \frac{1}{N_{\text{MC}}} \sum_{i=1}^{N_{\text{MC}}} \left(\frac{d\sigma}{d\Phi} \right)_i, \quad (4.10)$$

where N_{MC} is the number of events passing all selection criteria. For technical reasons, rather than maximizing \mathcal{L} , the object function, $S = -\ln \mathcal{L}$, is minimized using the package MINUIT [34]. To subtract background events, the likelihood function is calculated for both data ($\ln \mathcal{L}_{\text{data}}$) and background selected from the sideband regions ($\ln \mathcal{L}_{\text{bkg}}$), i.e.

$$S = -\ln \mathcal{L} = -\ln \mathcal{L}_{\text{data}} + \ln \mathcal{L}_{\text{bkg}}. \quad (4.11)$$

With the parameters obtained from the fit, the signal yield of a given resonance can be estimated as

$$N_i = \frac{\sigma_i(N_{\text{obs}} - N_{\text{bkg}})}{\sigma_{\text{tot}}}, \quad (4.12)$$

where σ_i is evaluated with the differential cross section for the i -th resonance, σ_{tot} is the total cross section including interference effects, $N_{\text{obs}} = 8664$ is the number of observed events, and $N_{\text{bkg}} = 166$ is the number of background events.

The statistical uncertainty δN_i associated with the signal yield N_i is estimated according to the error propagation formula using the covariance matrix V which is obtained in the MIGRAD fit,

$$\delta N_i^2 = \sum_{m=1}^{N_{\text{pars}}} \sum_{n=1}^{N_{\text{pars}}} \left(\frac{\partial N_i}{\partial X_m} \frac{\partial N_i}{\partial X_n} \right)_{X=\mu} V_{mn}(X), \quad (4.13)$$

where X is the vector parameters, and μ contains the fitted values for all parameters. The sum runs over all N_{pars} fit parameters.

4.5 Fit results

To consider the possible interference between the χ_{c0} and non-resonant $\phi\phi$ events, the latter are decomposed into their 0^+ and 0^- components. Since the χ_{c1} and χ_{c2} are quite narrow, their interference with a non-resonant contribution is neglected. Therefore, only the possible interference between the χ_{c0} and non-resonant contributions is considered. The mass and width of the χ_{c0} are free parameters in the fit, and they are determined to be $3415.42 \text{ MeV}/c^2$ and 11.4 MeV respectively, which are greater than the world average values ($3414.71 \pm 0.30 \text{ MeV}/c^2$ and $10.8 \pm 0.6 \text{ MeV}$) from ref. [22]. Meanwhile, the masses and widths of the χ_{c1} and χ_{c2} are fixed to the world average values, namely $M_{\chi_{c1}} = 3510.67 \text{ MeV}/c^2$, $\Gamma_{\chi_{c1}} = 0.84 \text{ MeV}$, $M_{\chi_{c2}} = 3556.17 \text{ MeV}/c^2$, and $\Gamma_{\chi_{c2}} = 1.97 \text{ MeV}$.

The $\phi\phi$ and $\gamma\phi$ invariant mass, as well as helicity angular distributions of γ and ϕ , are shown in figure 3 and figure 4, respectively.

With the fitted parameters, the fractions of signal yields in eq. (4.12) are determined to be $(31.79 \pm 0.99)\%$, $(17.99 \pm 0.53)\%$, and $(49.98 \pm 1.09)\%$ for the decay $\psi(3686) \rightarrow \gamma\chi_{cJ}$ followed by $\chi_{cJ} \rightarrow \phi\phi$ ($J = 0, 1, 2$), respectively. The ratio of amplitude moduli for $\chi_{c0} \rightarrow \phi\phi$ is determined to be

$$x = \left| F_{1,1}^0 \right| / \left| F_{0,0}^0 \right| = 0.299 \pm 0.003. \quad (4.14)$$

For $\chi_{c1} \rightarrow \phi\phi$, the ratios of amplitude moduli are determined to be

$$u_1 = |F_{1,0}^1/F_{0,1}^1| = 1.05 \pm 0.05 \text{ and } u_2 = |F_{1,1}^1/F_{1,0}^1| = 0.07 \pm 0.04. \quad (4.15)$$

These two ratios are well consistent with the expectation of identical particle symmetry and parity conservation in strong decays.

For $\chi_{c2} \rightarrow \phi\phi$, the ratios of amplitude moduli are calculated to be

$$\begin{aligned} \omega_1 &= \left| F_{0,1}^2 \right| / \left| F_{0,0}^2 \right| = 1.265 \pm 0.054, \\ \omega_2 &= \left| F_{1,-1}^2 \right| / \left| F_{0,0}^2 \right| = 1.450 \pm 0.097, \\ \omega_4 &= \left| F_{1,1}^2 \right| / \left| F_{0,0}^2 \right| = 0.808 \pm 0.051, \end{aligned} \quad (4.16)$$

where the uncertainties are statistical only.

The branching fractions for $\chi_{cJ} \rightarrow \phi\phi$ are determined by

$$\mathcal{B}[\chi_{cJ} \rightarrow \phi\phi] = \frac{N}{\epsilon * N_{\psi(3686)} * \mathcal{B}[\psi(3686) \rightarrow \gamma\chi_{cJ}] * \mathcal{B}^2[\phi \rightarrow K^+K^-]}, \quad (4.17)$$

where N is χ_{cJ} signal yield which has been defined in eq. (4.12), $N_{\psi(3686)}$ is the number of $\psi(3686)$ events [13], ϵ is efficiency, $\mathcal{B}[\psi(3686) \rightarrow \gamma\chi_{cJ}]$ and $\mathcal{B}[\phi \rightarrow K^+K^-]$ is the branching fractions for $\psi(3686) \rightarrow \gamma\chi_{cJ}$ and $\phi \rightarrow K^+K^-$ quoted from ref. [22], respectively. The branching fractions for $\chi_{cJ} \rightarrow \phi\phi$ with statistical uncertainties only and the parameters involved in calculation are summarized in table 4.

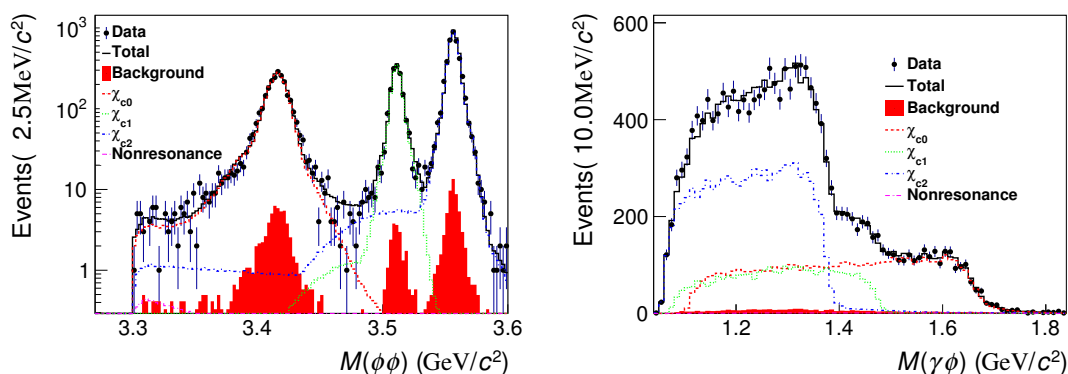


Figure 3. Fit results of invariant mass distributions, $m_{\phi\phi}$ in the log version (left) and $m_{\gamma\phi}$ (right). The points with error bars represent data events. The black solid curve denotes the total fit result. The $m_{\gamma\phi}$ distribution has two entries per event. Distributions of non-resonant events are almost invisible owing to the small contribution of this component.

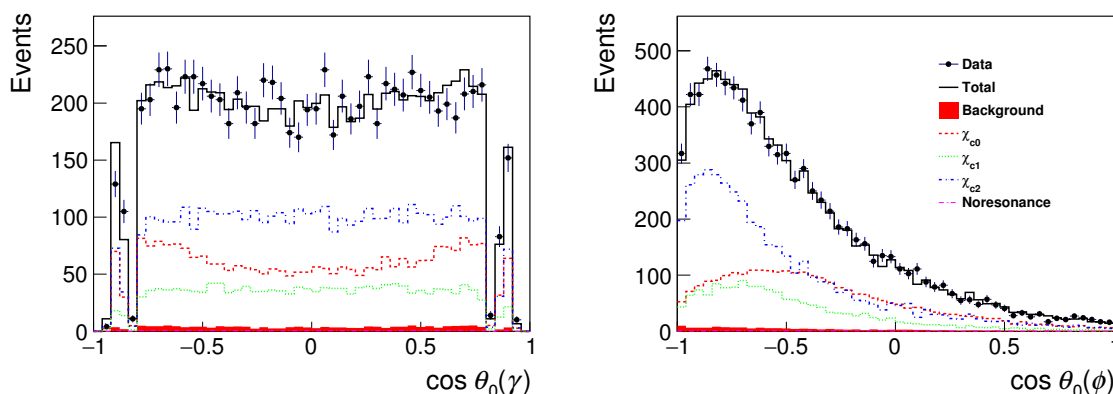


Figure 4. Fit results of helicity angular distributions for the photon (left) and the ϕ meson (right). The points with error bars represent data events; the black solid curve denotes the total fit result. The red dashed, green dotted, and blue dashed-dotted curves represent the χ_{c0} , χ_{c1} and χ_{c2} components, respectively.

Channel	$\chi_{c0} \rightarrow \phi\phi$	$\chi_{c1} \rightarrow \phi\phi$	$\chi_{c2} \rightarrow \phi\phi$
N	2701 ± 84	1529 ± 45	4247 ± 93
$\epsilon(\%)$	29.73 ± 0.10	34.09 ± 0.10	32.60 ± 0.10
$N_{\psi(3686)} (\times 10^6)$	447.9 ± 2.9	447.9 ± 2.9	447.9 ± 2.9
$\mathcal{B}(\psi(3686) \rightarrow \gamma\chi_{cJ}) (\%)$	9.79 ± 0.20	9.75 ± 0.24	9.52 ± 0.20
$\mathcal{B}(\phi \rightarrow K^+K^-) (\%)$	49.1 ± 0.5	49.1 ± 0.5	49.1 ± 0.5
$\mathcal{B}(\chi_{cJ} \rightarrow \phi\phi) (\times 10^{-4})$	8.59 ± 0.27	4.26 ± 0.13	12.67 ± 0.28

Table 4. Summary of the branching fractions for $\chi_{cJ} \rightarrow \phi\phi$ and the parameters included in calculation.

5 Systematic uncertainties

The systematic uncertainties of helicity amplitude measurements are associated with the value of Blatt-Weisskopf barrier factor d , the tracking efficiency, the photon detection, the kinematic fit, the background estimation, and the mass resolution. Additionally, the number of $\psi(3686)$ events represents a source of uncertainty for the branching fraction determination.

- *Branching fraction of intermediate states.* Branching fraction uncertainties for the decays $\mathcal{B}(\psi(3686) \rightarrow \gamma\chi_{c0})$, $\mathcal{B}(\psi(3686) \rightarrow \gamma\chi_{c1})$, $\mathcal{B}(\psi(3686) \rightarrow \gamma\chi_{c2})$, and $\mathcal{B}(\phi \rightarrow K^+K^-)$ are equal, respectively, to 2.0%, 2.5%, 2.1%, and 1.0% ref. [22].
- *Blatt-Weisskopf barrier factor d .* The systematic uncertainty arising from this term is determined via varying the factor d between 1.5 and 4.5 GeV^{-1} . The largest deviation from the nominal fit is determined to be 0.31%, which is negligible.
- *Tracking efficiency and photon reconstruction.* Tracking efficiencies for charged kaons are determined with a control sample of $J/\psi \rightarrow K^-K^{*+}$, $K^{*+} \rightarrow K^+\pi^0$ for K^+ and $J/\psi \rightarrow K^+K^{*-}$, $K^{*-} \rightarrow K^-\pi^0$ for K^- , respectively [8]. The uncertainty due to the photon reconstruction is determined using a control sample of $J/\psi \rightarrow \rho^0\pi^0 \rightarrow \pi^+\pi^-\gamma\gamma$ [35]. The ratio of efficiencies between data and MC simulation, $r(p_t, \cos\theta) = \epsilon_{\text{data}}(p_t, \cos\theta)/\epsilon_{\text{MC}}(p_t, \cos\theta)$, is taken as a factor to weight the squared amplitude of MC events to match that of data events dependent on the transverse momentum and polar angle of the track or shower. The difference of results with or without the weighting factor is taken as the systematic uncertainty.
- *Kinematic fit.* The systematic uncertainty from the kinematic fit is caused by the discrepancy between data and MC simulation in shower parameters for photons and track parameters for charged tracks. The simulation of photons has been investigated in ref. [35], which shows good agreement between data and MC simulation. For the charged tracks, the track helix parameter correction method [36, 37] is used. The systematic uncertainty is determined by replacing the MC sample with the helix-parameter-corrected ones when calculating the σ_{MC} .
- *χ_{c1} and χ_{c2} masses and widths.* Alternative fits are performed where the resonance parameters of χ_{c1} and χ_{c2} are fixed to the values sampled within one standard deviation of the PDG values [22]. The resultant differences from the nominal fit are taken as the systematic uncertainties.
- *Mass resolution.* The uncertainty of the mass resolution is determined by replacing the resolution functions obtained from the signal MC samples with the new one obtained from the control samples in data.
- *Background estimation.* The number of background events, estimated to be $N_{\text{bkg}} = 166 \pm 13$, is subtracted in the fit. The systematic uncertainty due to the background fluctuation is estimated by assuming a Gaussian distribution, $G(N_{\text{bkg}}, \delta N_{\text{bkg}})$, whose

width is $\delta N_{\text{bkg}} = 13$, which is taken as a new weighting factor propagated to amplitude model by modifying the log-likelihood function as $G(N_{\text{bkg}}, \delta N_{\text{bkg}}) \ln \mathcal{L}_{\text{bkg}}$.

- *Number of $\psi(3686)$ events.* The number of $\psi(3686)$ events is measured by studying inclusive hadronic decays. The uncertainty is about 0.6% [13].
- The possible correlations among the tracking efficiency, photon reconstruction, kinematic fit calculation, χ_{c1} and χ_{c2} masses and widths, mass resolution discrepancy and background estimation are considered in alternative fits. The normalization factor σ_{MC} in eq. (4.10) is modified as

$$\sigma_{\text{MC}} = \frac{1}{N_{\text{MC}}} \sum_{i=1}^{N_{\text{MC}}} \sum_{j=1}^{N_{\text{MC}}} |\mathcal{M}(\chi_{c0}) + \mathcal{M}(\chi_{c1}) + \mathcal{M}(\chi_{c2}) + \mathcal{M}(NR)|^2 T_{\text{corr}}, \quad (5.1)$$

where the factor T_{corr} is defined as the product of the correction factors for the γ and $2(K^+K^-)$ tracking ratios, $r(p_t, \cos \theta)$, for a given event, and the masses and widths of χ_{c1} and χ_{c2} are sampled within one standard deviation of the PDG values [22]. The mass resolution function for χ_{c0} is replaced by the alternative one. The MC events are replaced by the helix-parameter-corrected ones. Then alternative fits are performed to obtain the χ_{cJ} helicity amplitude ratios, the mass and width of χ_{c0} , and the signal yields for each resonance. The differences with individual nominal results are taken as the correlated systematic uncertainties of the amplitude analysis, as given in table 5. It is notable that the determined uncertainty for the ratio of amplitude moduli of the helicity conserved amplitudes ($|F_{1,1}^2| / |F_{0,0}^2|$) is smaller than those of the other helicity violated amplitudes. This is due to the fact that in the helicity conserving amplitude, the kinematic fit and other systematic errors have opposite signs and cancel each other, while in the helicity violating amplitude, the signs are the same and the errors are constructive.

6 Conclusion and discussion

Using (447.9 ± 2.3) million $\psi(3686)$ events collected with the BESIII detector, the helicity amplitudes for the decays $\psi(3686) \rightarrow \gamma\chi_{cJ}$, $\chi_{cJ} \rightarrow \phi\phi$, and $\phi \rightarrow K^+K^-$ are studied.

The branching fractions for $\chi_{cJ} \rightarrow \phi\phi$ are measured to be

$$\begin{aligned} \mathcal{B}(\chi_{c0} \rightarrow \phi\phi) &= (8.59 \pm 0.27 \pm 0.20) \times 10^{-4}, \\ \mathcal{B}(\chi_{c1} \rightarrow \phi\phi) &= (4.26 \pm 0.13 \pm 0.15) \times 10^{-4}, \\ \mathcal{B}(\chi_{c2} \rightarrow \phi\phi) &= (12.67 \pm 0.28 \pm 0.33) \times 10^{-4}, \end{aligned} \quad (6.1)$$

where the first uncertainties are statistical and the second systematic. Comparing these results with BESIII previous measurement [8] and PDG values [22], as reflected in the table 6, the precision is improved by a factor of about 2, but the values are greater.

The ratios of the amplitude moduli are measured to be

$$\left| F_{1,1}^0 \right| / \left| F_{0,0}^0 \right| = 0.299 \pm 0.003 \pm 0.019, \quad (6.2)$$

Source	$\mathcal{B}(\chi_{c0})$	$\mathcal{B}(\chi_{c1})$	$\mathcal{B}(\chi_{c2})$	
$N_{\psi(3686)}$	0.6%	0.6%	0.6%	
$\mathcal{B}(\psi(3686) \rightarrow \gamma\chi_{cJ})$	2.0%	2.5%	2.1%	
$\mathcal{B}(\phi \rightarrow K^+K^-)$	1.0%	1.0%	1.0%	
Correlated sources	0.4%	2.3%	1.1%	
Total	2.3%	3.5%	2.6%	
Sources	$\frac{ F_{1,1}^0 }{ F_{0,0}^0 }$	$\frac{ F_{0,1}^2 }{ F_{0,0}^2 }$	$\frac{ F_{1,-1}^2 }{ F_{0,0}^2 }$	$\frac{ F_{1,1}^2 }{ F_{0,0}^2 }$
$N_{\psi(3686)}$	—	—	—	—
$\mathcal{B}(\psi(3686) \rightarrow \gamma\chi_{cJ})$	—	—	—	—
$\mathcal{B}(\phi \rightarrow K^+K^-)$	—	—	—	—
Correlated sources	6.4%	6.2%	7.1%	1.1%
Total	6.4%	6.2%	7.1%	1.1%

Table 5. Summary of systematic uncertainties. The correlated sources include the tracking efficiency, photon reconstruction, kinematic fit, backgrounds, χ_{c1} and χ_{c2} masses and widths and mass resolution. $\mathcal{B}(\chi_{cJ})$ denotes the branching fraction for $\chi_{cJ} \rightarrow \phi\phi$. The “—” means that this term is not entering in the corresponding measurement.

Decay Mode	2011 BESIII [8]	this work	PDG value [22]
$\mathcal{B}[\chi_{c0} \rightarrow \phi\phi](\times 10^{-4})$	$7.8 \pm 0.4 \pm 0.8$	$8.59 \pm 0.27 \pm 0.20$	8.0 ± 0.7
$\mathcal{B}[\chi_{c1} \rightarrow \phi\phi](\times 10^{-4})$	$4.1 \pm 0.3 \pm 0.5$	$4.26 \pm 0.13 \pm 0.15$	4.2 ± 0.5
$\mathcal{B}[\chi_{c1} \rightarrow \phi\phi](\times 10^{-4})$	$10.7 \pm 0.4 \pm 1.2$	$12.67 \pm 0.28 \pm 0.33$	10.6 ± 0.9

Table 6. Comparison of measured branching fractions (\mathcal{B}).

for $\chi_{c0} \rightarrow \phi\phi$, and

$$\left| \frac{F_{0,1}^2}{F_{0,0}^2} \right| / \left| \frac{F_{0,0}^2}{F_{0,0}^2} \right| = 1.265 \pm 0.054 \pm 0.079, \quad (6.3)$$

$$\left| \frac{F_{1,-1}^2}{F_{0,0}^2} \right| / \left| \frac{F_{0,0}^2}{F_{0,0}^2} \right| = 1.450 \pm 0.097 \pm 0.104, \quad (6.4)$$

$$\left| \frac{F_{1,1}^2}{F_{0,0}^2} \right| / \left| \frac{F_{0,0}^2}{F_{0,0}^2} \right| = 0.808 \pm 0.051 \pm 0.009, \quad (6.5)$$

for $\chi_{c2} \rightarrow \phi\phi$, where the first and second uncertainties are statistical and systematic, respectively. Additionally, there is no evidence of identical particle symmetry breaking from the study of $\chi_{c1} \rightarrow \phi\phi$.

Figure 5 shows a comparison of the measured amplitude ratios to the corresponding theoretical predictions. The measured ratio of amplitude moduli for the χ_{c0} is consistent with the pQCD prediction of ref. [6], since two independent helicity amplitudes of the $\chi_{c0} \rightarrow \phi\phi$ decay, $F_{1,1}^0$ and $F_{0,0}^0$, follow the helicity selection rule. For the χ_{c2} decay, the measured ratios of amplitude moduli deviate from the pQCD [6], 3P_0 [9] and $D\bar{D}$ loop [10]

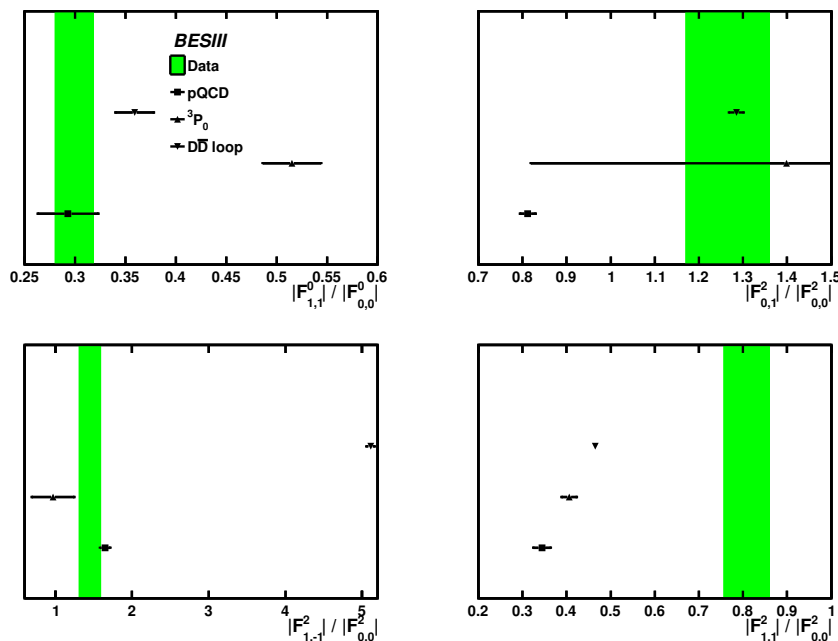


Figure 5. Comparison of the measured amplitude ratios with the predicted ones from pQCD, the 3P_0 model and the $D\bar{D}$ loop model.

predictions with $\chi^2/\text{ndf} = 23.2, 23.8,$ and $155.2,$ respectively. The $D\bar{D}$ loop model can be ruled out due to the large deviation. However, the predictions of other models also differ from the experimental results. In short, all of the above theories use some of the input from the experimental results, thus this measurement can provide more constraints for further developing the models. It could also be a basis for the measurement in the future, as 2.7 billion $\psi(3686)$ events have been accumulated in BESIII [38].

Acknowledgments

The BESIII collaboration thanks the staff of BEPCII and the IHEP computing center for their strong support. This work is supported in part by National Key R&D Program of China under Contracts Nos. 2020YFA0406300, 2020YFA0406400; National Natural Science Foundation of China (NSFC) under Contracts Nos. 11875262, 12175244, 11635010, 11735014, 11835012, 11935015, 11935016, 11935018, 11961141012, 12022510, 12025502, 12035009, 12035013, 12192260, 12192261, 12192262, 12192263, 12192264, 12192265; the Chinese Academy of Sciences (CAS) Large-Scale Scientific Facility Program; Joint Large-Scale Scientific Facility Funds of the NSFC and CAS under Contract No. U1832207, U2032110; CAS Key Research Program of Frontier Sciences under Contract No. QYZDJJ-SSW-SLH040; 100 Talents Program of CAS; The Institute of Nuclear and Particle Physics (INPAC) and Shanghai Key Laboratory for Particle Physics and Cosmology; ERC under Contract No. 758462; European Union’s Horizon 2020 research and innovation programme under Marie Skłodowska-Curie grant agreement under Contract No. 894790; German Research Foundation DFG under Contracts Nos. 443159800, Collaborative Research Center CRC

1044, GRK 2149; Istituto Nazionale di Fisica Nucleare, Italy; Ministry of Development of Turkey under Contract No. DPT2006K-120470; National Science and Technology fund; National Science Research and Innovation Fund (NSRF) via the Program Management Unit for Human Resources & Institutional Development, Research and Innovation under Contract No. B16F640076; STFC (United Kingdom); Suranaree University of Technology (SUT), Thailand Science Research and Innovation (TSRI), and National Science Research and Innovation Fund (NSRF) under Contract No. 160355; The Royal Society, U.K. under Contracts Nos. DH140054, DH160214; The Swedish Research Council; U.S. Department of Energy under Contract No. DE-FG02-05ER41374

Open Access. This article is distributed under the terms of the Creative Commons Attribution License ([CC-BY 4.0](https://creativecommons.org/licenses/by/4.0/)), which permits any use, distribution and reproduction in any medium, provided the original author(s) and source are credited. SCOAP³ supports the goals of the International Year of Basic Sciences for Sustainable Development.

References

- [1] A. Duncan and A.H. Mueller, *Heavy Quarkonium Decays and the Renormalization Group*, *Phys. Lett. B* **93** (1980) 119 [[INSPIRE](#)].
- [2] H.F. Jones and J. Wyndham, *Perturbative QCD and the Exclusive Decay of Heavy Quarkonium Into a Photon and Two Mesons*, *Nucl. Phys. B* **195** (1982) 222 [[INSPIRE](#)].
- [3] M. Anselmino and F. Murgia, $\chi_{c0,c2} \rightarrow \rho\rho$ decays and the ρ polarization: Massless versus constituent quarks, *Phys. Rev. D* **47** (1993) 3977 [[INSPIRE](#)].
- [4] V.L. Chernyak and A.R. Zhitnitsky, *Exclusive Decays of Heavy Mesons*, *Nucl. Phys. B* **201** (1982) 492 [*Erratum ibid.* **214** (1983) 547] [[INSPIRE](#)].
- [5] S.J. Brodsky and G.P. Lepage, *Helicity Selection Rules and Tests of Gluon Spin in Exclusive QCD Processes*, *Phys. Rev. D* **24** (1981) 2848 [[INSPIRE](#)].
- [6] H.Q. Zhou, R.G. Ping and B.S. Zou, *Mechanisms for $\chi_{cJ} \rightarrow \phi\phi$ decays*, *Phys. Lett. B* **611** (2005) 123 [[hep-ph/0412221](#)] [[INSPIRE](#)].
- [7] C.-N. Yang, *Selection Rules for the Dematerialization of a Particle Into Two Photons*, *Phys. Rev.* **77** (1950) 242 [[INSPIRE](#)].
- [8] BESII collaboration, *Observation of χ_{c1} decays into vector meson pairs $\phi\phi$, $\omega\omega$, and $\omega\phi$* , *Phys. Rev. Lett.* **107** (2011) 092001 [[arXiv:1104.5068](#)] [[INSPIRE](#)].
- [9] H. Chen and R.-G. Ping, *Polarization in $\chi_{cJ} \rightarrow \phi\phi$ decays*, *Phys. Rev. D* **88** (2013) 034025 [[INSPIRE](#)].
- [10] Q. Huang, J.-Z. Wang, R.-G. Ping and X. Liu, *Detecting the polarization in $\chi_{cJ} \rightarrow \phi\phi$ decays to probe hadronic loop effect*, *Phys. Rev. D* **103** (2021) 096006 [[arXiv:2102.07104](#)] [[INSPIRE](#)].
- [11] X.-H. Liu and Q. Zhao, *The Evasion of helicity selection rule in $\chi_{c1} \rightarrow VV$ and $\chi_{c2} \rightarrow VP$ via intermediate charmed meson loops*, *Phys. Rev. D* **81** (2010) 014017 [[arXiv:0912.1508](#)] [[INSPIRE](#)].
- [12] D.-Y. Chen, J. He, X.-Q. Li and X. Liu, *Understanding the branching ratios of $\chi_{c1} \rightarrow \phi\phi$, $\omega\omega$, $\omega\phi$ observed at BES-III*, *Phys. Rev. D* **81** (2010) 074006 [[arXiv:0912.4860](#)] [[INSPIRE](#)].

- [13] BESIII collaboration, *Determination of the number of $\psi(3686)$ events at BESIII*, *Chin. Phys. C* **42** (2018) 023001 [[arXiv:1709.03653](#)] [[INSPIRE](#)].
- [14] BESIII collaboration, *Design and Construction of the BESIII Detector*, *Nucl. Instrum. Meth. A* **614** (2010) 345 [[arXiv:0911.4960](#)] [[INSPIRE](#)].
- [15] R. Palmer et al., *Higher Luminosity eRHIC Ring-Ring Options and Upgrade*, in the proceedings of the *7th International Particle Accelerator Conference*, Busan, Korea (2016), p. WEPMW023 [[DOI:10.18429/JACoW-IPAC2016-WEPMW023](#)] [[INSPIRE](#)].
- [16] K.-X. Huang et al., *Method for detector description transformation to Unity and application in BESIII*, *Nucl. Sci. Tech.* **33** (2022) 142 [[arXiv:2206.10117](#)] [[INSPIRE](#)].
- [17] GEANT4 collaboration, *Geant4 — a simulation toolkit*, *Nucl. Instrum. Meth. A* **506** (2003) 250 [[INSPIRE](#)].
- [18] S. Jadach, B.F.L. Ward and Z. Was, *Coherent exclusive exponentiation for precision Monte Carlo calculations*, *Nucl. Phys. B Proc. Suppl.* **89** (2000) 106 [[hep-ph/0012124](#)] [[INSPIRE](#)].
- [19] S. Jadach, B.F.L. Ward and Z. Was, *The Precision Monte Carlo event generator KK for two fermion final states in e^+e^- collisions*, *Comput. Phys. Commun.* **130** (2000) 260 [[hep-ph/9912214](#)] [[INSPIRE](#)].
- [20] D.J. Lange, *The EvtGen particle decay simulation package*, *Nucl. Instrum. Meth. A* **462** (2001) 152 [[INSPIRE](#)].
- [21] R.-G. Ping, *Event generators at BESIII*, *Chin. Phys. C* **32** (2008) 599 [[INSPIRE](#)].
- [22] PARTICLE DATA GROUP collaboration, *Review of Particle Physics*, *PTEP* **2022** (2022) 083C01 [[INSPIRE](#)].
- [23] J.C. Chen et al., *Event generator for J/ψ and $\psi(2S)$ decay*, *Phys. Rev. D* **62** (2000) 034003 [[INSPIRE](#)].
- [24] R.-L. Yang, R.-G. Ping and H. Chen, *Tuning and Validation of the Lundcharm Model with J/ψ Decays*, *Chin. Phys. Lett.* **31** (2014) 061301 [[INSPIRE](#)].
- [25] E. Richter-Was, *QED bremsstrahlung in semileptonic B and leptonic tau decays*, *Phys. Lett. B* **303** (1993) 163 [[INSPIRE](#)].
- [26] X. Zhou, S. Du, G. Li and C. Shen, *TopoAna: A generic tool for the event type analysis of inclusive Monte-Carlo samples in high energy physics experiments*, *Comput. Phys. Commun.* **258** (2021) 107540 [[arXiv:2001.04016](#)] [[INSPIRE](#)].
- [27] S.U. Chung, *A General formulation of covariant helicity coupling amplitudes*, *Phys. Rev. D* **57** (1998) 431 [[INSPIRE](#)].
- [28] S.U. Chung, *Helicity coupling amplitudes in tensor formalism*, *Phys. Rev. D* **48** (1993) 1225 [*Erratum ibid.* **56** (1997) 4419] [[INSPIRE](#)].
- [29] S.-U. Chung and J. Friedrich, *Covariant helicity-coupling amplitudes: A New formulation*, *Phys. Rev. D* **78** (2008) 074027 [[arXiv:0711.3143](#)] [[INSPIRE](#)].
- [30] S.U. Chung, *Spin formalisms*, CERN-71-08 (1971) [[DOI:10.5170/CERN-1971-008](#)] [[INSPIRE](#)].
- [31] V. Filippini, A. Fontana and A. Rotondi, *Covariant spin tensors in meson spectroscopy*, *Phys. Rev. D* **51** (1995) 2247 [[INSPIRE](#)].
- [32] B.S. Zou and D.V. Bugg, *Covariant tensor formalism for partial wave analyses of psi decay to mesons*, *Eur. Phys. J. A* **16** (2003) 537 [[hep-ph/0211457](#)] [[INSPIRE](#)].

- [33] LHCb collaboration, *Observation of $J/\psi p$ Resonances Consistent with Pentaquark States in $\Lambda_b^0 \rightarrow J/\psi K^- p$ Decays*, *Phys. Rev. Lett.* **115** (2015) 072001 [[arXiv:1507.03414](#)] [[INSPIRE](#)].
- [34] ROOT Reference Documentation, <https://cdsweb.cern.ch/record/2296388/files/minuit.pdf>.
- [35] BESIII collaboration, *Branching fraction measurements of χ_{c0} and χ_{c2} to $\pi^0\pi^0$ and $\eta\eta$* , *Phys. Rev. D* **81** (2010) 052005 [[arXiv:1001.5360](#)] [[INSPIRE](#)].
- [36] BESIII collaboration, *Search for hadronic transition $\chi_{cJ} \rightarrow \eta_c \pi^+ \pi^-$ and observation of $\chi_{cJ} \rightarrow K\bar{K}\pi\pi\pi$* , *Phys. Rev. D* **87** (2013) 012002 [[arXiv:1208.4805](#)] [[INSPIRE](#)].
- [37] BESIII collaboration, *Observation of h_c radiative decay $h_c \rightarrow \gamma\eta'$ and evidence for $h_c \rightarrow \gamma\eta$* , *Phys. Rev. Lett.* **116** (2016) 251802 [[arXiv:1603.04936](#)] [[INSPIRE](#)].
- [38] BESIII collaboration, *Future Physics Programme of BESIII*, *Chin. Phys. C* **44** (2020) 040001 [[arXiv:1912.05983](#)] [[INSPIRE](#)].

The ANTARES collaboration

M. Ablikim¹, M.N. Achasov^{11,b}, P. Adlarson⁷⁰, M. Albrecht⁴, R. Aliberti³¹, A. Amoroso^{69A,69C}, M.R. An³⁵, Q. An^{66,53}, X.H. Bai⁶¹, Y. Bai⁵², O. Bakina³², R. Baldini Ferroli^{26A}, I. Balossino^{27A}, Y. Ban^{42,g}, V. Batozskaya^{1,40}, D. Becker³¹, K. Begzsuren²⁹, N. Berger³¹, M. Bertani^{26A}, D. Bettoni^{27A}, F. Bianchi^{69A,69C}, J. Bloms⁶³, A. Bortone^{69A,69C}, I. Boyko³², R.A. Briere⁵, A. Brueggemann⁶³, H. Cai⁷¹, X. Cai^{1,53}, A. Calcaterra^{26A}, G.F. Cao^{1,58}, N. Cao^{1,58}, S.A. Cetin^{57A}, J.F. Chang^{1,53}, W.L. Chang^{1,58}, G. Chelkov^{32,a}, C. Chen³⁹, Chao Chen⁵⁰, G. Chen¹, H.S. Chen^{1,58}, M.L. Chen^{1,53}, S.J. Chen³⁸, S.M. Chen⁵⁶, T. Chen¹, X.R. Chen^{28,58}, X.T. Chen¹, Y.B. Chen^{1,53}, Z.J. Chen^{23,h}, W.S. Cheng^{69C}, S.K. Choi⁵⁰, X. Chu³⁹, G. Cibinetto^{27A}, F. Cossio^{69C}, J.J. Cui⁴⁵, H.L. Dai^{1,53}, J.P. Dai⁷³, A. Dbeyssi¹⁷, R.E. de Boer⁴, D. Dedovich³², Z.Y. Deng¹, A. Denig³¹, I. Denysenko³², M. Destefanis^{69A,69C}, F. De Mori^{69A,69C}, Y. Ding³⁶, J. Dong^{1,53}, L.Y. Dong^{1,58}, M.Y. Dong^{1,53,58}, X. Dong⁷¹, S.X. Du⁷⁵, P. Egorov^{32,a}, Y.L. Fan⁷¹, J. Fang^{1,53}, S.S. Fang^{1,58}, W.X. Fang¹, Y. Fang¹, R. Farinelli^{27A}, L. Fava^{69B,69C}, F. Feldbauer⁴, G. Felici^{26A}, C.Q. Feng^{66,53}, J.H. Feng⁵⁴, K. Fischer⁶⁴, M. Fritsch⁴, C. Fritzschn⁶³, C.D. Fu¹, H. Gao⁵⁸, Y.N. Gao^{42,g}, Yang Gao^{66,53}, S. Garbolino^{69C}, I. Garzia^{27A,27B}, P.T. Ge⁷¹, Z.W. Ge³⁸, C. Geng⁵⁴, E.M. Gersabeck⁶², A. Gilman⁶⁴, K. Goetzen¹², L. Gong³⁶, W.X. Gong^{1,53}, W. Gradl³¹, M. Greco^{69A,69C}, L.M. Gu³⁸, M.H. Gu^{1,53}, Y.T. Gu¹⁴, C. Y Guan^{1,58}, A.Q. Guo^{28,58}, L.B. Guo³⁷, R.P. Guo⁴⁴, Y.P. Guo^{10,f}, A. Guskov^{32,a}, T.T. Han⁴⁵, W.Y. Han³⁵, X.Q. Hao¹⁸, F.A. Harris⁶⁰, K.K. He⁵⁰, K.L. He^{1,58}, F.H. Heinsius⁴, C.H. Heinz³¹, Y.K. Heng^{1,53,58}, C. Herold⁵⁵, M. Himmelreich^{31,d}, G.Y. Hou^{1,58}, Y.R. Hou⁵⁸, Z.L. Hou¹, H.M. Hu^{1,58}, J.F. Hu^{51,i}, T. Hu^{1,53,58}, Y. Hu¹, G.S. Huang^{66,53}, K.X. Huang⁵⁴, L.Q. Huang^{28,58}, L.Q. Huang⁶⁷, X.T. Huang⁴⁵, Y.P. Huang¹, Z. Huang^{42,g}, T. Hussain⁶⁸, N. Hüskens^{25,31}, W. Imoehl²⁵, M. Irshad^{66,53}, J. Jackson²⁵, S. Jaeger⁴, S. Janchiv²⁹, E. Jang⁵⁰, J.H. Jeong⁵⁰, Q. Ji¹, Q.P. Ji¹⁸, X.B. Ji^{1,58}, X.L. Ji^{1,53}, Y.Y. Ji⁴⁵, Z.K. Jia^{66,53}, H.B. Jiang⁴⁵, S.S. Jiang³⁵, X.S. Jiang^{1,53,58}, Y. Jiang⁵⁸, J.B. Jiao⁴⁵, Z. Jiao²¹, S. Jin³⁸, Y. Jin⁶¹, M.Q. Jing^{1,58}, T. Johansson⁷⁰, N. Kalantar-Nayestanaki⁵⁹, X.S. Kang³⁶, R. Kappert⁵⁹, M. Kavatsyuk⁵⁹, B.C. Ke⁷⁵, I.K. Keshk⁴, A. Khoukaz⁶³, R. Kiuchi¹, R. Kliemt¹², L. Koch³³, O.B. Kolcu^{57A}, B. Kopf⁴, M. Kuemmel⁴, M. Kuessner⁴, A. Kupsc^{40,70}, W. Kühn³³, J.J. Lane⁶², J.S. Lange³³, P. Larin¹⁷, A. Lavania²⁴, L. Lavezzi^{69A,69C}, T.T. Lei^{66,k}, Z.H. Lei^{66,53}, H. Leithoff³¹, M. Lellmann³¹, T. Lenz³¹, C. Li³⁹, C. Li⁴³, C.H. Li³⁵, Cheng Li^{66,53}, D.M. Li⁷⁵, F. Li^{1,53}, G. Li¹, H. Li⁴⁷, H. Li^{66,53}, H.B. Li^{1,58}, H.J. Li¹⁸, H.N. Li^{51,i}, J.Q. Li⁴, J.S. Li⁵⁴, J.W. Li⁴⁵, Ke Li¹, L. J Li¹, L.K. Li¹, Lei Li³, M.H. Li³⁹, P.R. Li^{34,j,k}, S.X. Li¹⁰, S.Y. Li⁵⁶, T. Li⁴⁵, W.D. Li^{1,58}, W.G. Li¹, X.H. Li^{66,53}, X.L. Li⁴⁵, Xiaoyu Li^{1,58}, Z.X. Li¹⁴, Z.Y. Li⁵⁴, H. Liang^{66,53}, H. Liang³⁰, H. Liang^{1,58}, Y.F. Liang⁴⁹, Y.T. Liang^{28,58}, G.R. Liao¹³, L.Z. Liao⁴⁵, J. Libby²⁴, A. Limphirat⁵⁵, C.X. Lin⁵⁴, D.X. Lin^{28,58}, T. Lin¹, B.J. Liu¹, C.X. Liu¹, D. Liu^{17,66}, F.H. Liu⁴⁸, Fang Liu¹, Feng Liu⁶, G.M. Liu^{51,i}, H. Liu^{34,j,k}, H.B. Liu¹⁴, H.M. Liu^{1,58}, Huanhuan Liu¹, Huihui Liu¹⁹, J.B. Liu^{66,53}, J.L. Liu⁶⁷, J.Y. Liu^{1,58}, K. Liu¹, K.Y. Liu³⁶, Ke Liu²⁰, L. Liu^{66,53}, Lu Liu³⁹, M.H. Liu^{10,f}, P.L. Liu¹, Q. Liu⁵⁸, S.B. Liu^{66,53}, T. Liu^{10,f}, W.K. Liu³⁹, W.M. Liu^{66,53}, X. Liu^{34,j,k}, Y. Liu^{34,j,k}, Y.B. Liu³⁹, Z.A. Liu^{1,53,58}, Z.Q. Liu⁴⁵, X.C. Lou^{1,53,58}, F.X. Lu⁵⁴, H.J. Lu²¹, J.G. Lu^{1,53}, X.L. Lu¹, Y. Lu⁷, Y.P. Lu^{1,53}, Z.H. Lu¹, C.L. Luo³⁷, M.X. Luo⁷⁴, T. Luo^{10,f}, X.L. Luo^{1,53}, X.R. Lyu⁵⁸, Y.F. Lyu³⁹, F.C. Ma³⁶, H.L. Ma¹, L.L. Ma⁴⁵, M.M. Ma^{1,58}, Q.M. Ma¹, R.Q. Ma^{1,58}, R.T. Ma⁵⁸, X.Y. Ma^{1,53}, Y. Ma^{42,g}, F.E. Maas¹⁷, M. Maggiora^{69A,69C}, S. Maldaner⁴, S. Malde⁶⁴, Q.A. Malik⁶⁸, A. Mangoni^{26B}, Y.J. Mao^{42,g}, Z.P. Mao¹, S. Marcello^{69A,69C}, Z.X. Meng⁶¹, J.G. Messchendorp^{12,59}, G. Mezzadri^{27A}, H. Miao¹, T.J. Min³⁸, R.E. Mitchell²⁵, X.H. Mo^{1,53,58}, N. Yu. Muchnoi^{11,b}, Y. Nefedov³², F. Nerling^{17,d}, I.B. Nikolaev^{11,b}, Z. Ning^{1,53}, S. Nisar^{9,l}, Y. Niu⁴⁵, S.L. Olsen⁵⁸, Q. Ouyang^{1,53,58}, S. Pacetti^{26B,26C}, X. Pan^{10,f}, Y. Pan⁵², A. Pathak³⁰, Y.P. Pei^{66,53}, M. Pelizaeus⁴, H.P. Peng^{66,53}, K. Peters^{12,d}, J.L. Ping³⁷, R.G. Ping^{1,58}, S. Plura³¹, S. Pogodin³², V. Prasad^{66,53}, F.Z. Qi¹, H. Qi^{66,53}, H.R. Qi⁵⁶, M. Qi³⁸,

T.Y. Qi^{10,f}, S. Qian^{1,53}, W.B. Qian⁵⁸, Z. Qian⁵⁴, C.F. Qiao⁵⁸, J.J. Qin⁶⁷, L.Q. Qin¹³, X.P. Qin^{10,f}, X.S. Qin⁴⁵, Z.H. Qin^{1,53}, J.F. Qiu¹, S.Q. Qu⁵⁶, S.Q. Qu³⁹, K.H. Rashid⁶⁸, C.F. Redmer³¹, K.J. Ren³⁵, A. Rivetti^{69C}, V. Rodin⁵⁹, M. Rolo^{69C}, G. Rong^{1,58}, Ch. Rosner¹⁷, S.N. Ruan³⁹, A. Sarantsev^{32,c}, Y. Schelhaas³¹, C. Schnier⁴, K. Schoenning⁷⁰, M. Scodreggio^{27A,27B}, K.Y. Shan^{10,f}, W. Shan²², X.Y. Shan^{66,53}, J.F. Shangguan⁵⁰, L.G. Shao^{1,58}, M. Shao^{66,53}, C.P. Shen^{10,f}, H.F. Shen^{1,58}, X.Y. Shen^{1,58}, B.A. Shi⁵⁸, H.C. Shi^{66,53}, J.Y. Shi¹, q. q. Shi⁵⁰, R.S. Shi^{1,58}, X. Shi^{1,53}, X. D Shi^{66,53}, J.J. Song¹⁸, W.M. Song^{30,1}, Y.X. Song^{42,g}, S. Sosio^{69A,69C}, S. Spataro^{69A,69C}, F. Stieler³¹, K.X. Su⁷¹, P.P. Su⁵⁰, Y.J. Su⁵⁸, G.X. Sun¹, H. Sun⁵⁸, H.K. Sun¹, J.F. Sun¹⁸, L. Sun⁷¹, S.S. Sun^{1,58}, T. Sun^{1,58}, W.Y. Sun³⁰, X Sun^{23,h}, Y.J. Sun^{66,53}, Y.Z. Sun¹, Z.T. Sun⁴⁵, Y.H. Tan⁷¹, Y.X. Tan^{66,53}, C.J. Tang⁴⁹, G.Y. Tang¹, J. Tang⁵⁴, L. Y Tao⁶⁷, Q.T. Tao^{23,h}, M. Tat⁶⁴, J.X. Teng^{66,53}, V. Thoren⁷⁰, W.H. Tian⁴⁷, Y. Tian^{28,58}, I. Uman^{57B}, B. Wang^{66,53}, B. Wang¹, B.L. Wang⁵⁸, C.W. Wang³⁸, D.Y. Wang^{42,g}, F. Wang⁶⁷, H.J. Wang^{34,j,k}, H.P. Wang^{1,58}, K. Wang^{1,53}, L.L. Wang¹, M. Wang⁴⁵, M.Z. Wang^{42,g}, Meng Wang^{1,58}, S. Wang¹³, S. Wang^{10,f}, T. Wang^{10,f}, T.J. Wang³⁹, W. Wang⁵⁴, W.H. Wang⁷¹, W.P. Wang^{66,53}, X. Wang^{42,g}, X.F. Wang^{34,j,k}, X.L. Wang^{10,f}, Y. Wang⁵⁶, Y.D. Wang⁴¹, Y.F. Wang^{1,53,58}, Y.H. Wang⁴³, Y.Q. Wang¹, Yaqian Wang^{16,1}, Z. Wang^{1,53}, Z.Y. Wang^{1,58}, Ziyi Wang⁵⁸, D.H. Wei¹³, F. Weidner⁶³, S.P. Wen¹, D.J. White⁶², U. Wiedner⁴, G. Wilkinson⁶⁴, M. Wolke⁷⁰, L. Wollenberg⁴, J.F. Wu^{1,58}, L.H. Wu¹, L.J. Wu^{1,58}, X. Wu^{10,f}, X.H. Wu³⁰, Y. Wu⁶⁶, Y. J Wu²⁸, Z. Wu^{1,53}, L. Xia^{66,53}, T. Xiang^{42,g}, D. Xiao^{34,j,k}, G.Y. Xiao³⁸, H. Xiao^{10,f}, S.Y. Xiao¹, Y.L. Xiao^{10,f}, Z.J. Xiao³⁷, C. Xie³⁸, X.H. Xie^{42,g}, Y. Xie⁴⁵, Y.G. Xie^{1,53}, Y.H. Xie⁶, Z.P. Xie^{66,53}, T.Y. Xing^{1,58}, C.F. Xu¹, C.J. Xu⁵⁴, G.F. Xu¹, H.Y. Xu⁶¹, Q.J. Xu¹⁵, X.P. Xu⁵⁰, Y.C. Xu⁵⁸, Z.P. Xu³⁸, F. Yan^{10,f}, L. Yan^{10,f}, W.B. Yan^{66,53}, W.C. Yan⁷⁵, H.J. Yang^{46,e}, H.L. Yang³⁰, H.X. Yang¹, L. Yang⁴⁷, S.L. Yang⁵⁸, Tao Yang¹, Y.F. Yang³⁹, Y.X. Yang^{1,58}, Yifan Yang^{1,58}, M. Ye^{1,53}, M.H. Ye⁸, J.H. Yin¹, Z.Y. You⁵⁴, B.X. Yu^{1,53,58}, C.X. Yu³⁹, G. Yu^{1,58}, T. Yu⁶⁷, X.D. Yu^{42,g}, C.Z. Yuan^{1,58}, L. Yuan², S.C. Yuan¹, X.Q. Yuan¹, Y. Yuan^{1,58}, Z.Y. Yuan⁵⁴, C.X. Yue³⁵, A.A. Zafar⁶⁸, F.R. Zeng⁴⁵, X. Zeng⁶, Y. Zeng^{23,h}, Y.H. Zhan⁵⁴, A.Q. Zhang¹, B.L. Zhang¹, B.X. Zhang¹, D.H. Zhang³⁹, G.Y. Zhang¹⁸, H. Zhang⁶⁶, H.H. Zhang⁵⁴, H.H. Zhang³⁰, H.Y. Zhang^{1,53}, J.L. Zhang⁷², J.Q. Zhang³⁷, J.W. Zhang^{1,53,58}, J.X. Zhang^{34,j,k}, J.Y. Zhang¹, J.Z. Zhang^{1,58}, Jianyu Zhang^{1,58}, Jiawei Zhang^{1,58}, L.M. Zhang⁵⁶, L.Q. Zhang⁵⁴, Lei Zhang³⁸, P. Zhang¹, Q.Y. Zhang^{35,75}, Shuihan Zhang^{1,58}, Shulei Zhang^{23,h}, X.D. Zhang⁴¹, X.M. Zhang¹, X.Y. Zhang⁴⁵, X.Y. Zhang⁵⁰, Y. Zhang⁶⁴, Y.T. Zhang⁷⁵, Y.H. Zhang^{1,53}, Yan Zhang^{66,53}, Yao Zhang¹, Z.H. Zhang¹, Z.Y. Zhang³⁹, Z.Y. Zhang⁷¹, G. Zhao¹, J. Zhao³⁵, J.Y. Zhao^{1,58}, J.Z. Zhao^{1,53}, Lei Zhao^{66,53}, Ling Zhao¹, M.G. Zhao³⁹, Q. Zhao¹, S.J. Zhao⁷⁵, Y.B. Zhao^{1,53}, Y.X. Zhao^{28,58}, Z.G. Zhao^{66,53}, A. Zhemchugov^{32,a}, B. Zheng⁶⁷, J.P. Zheng^{1,53}, Y.H. Zheng⁵⁸, B. Zhong³⁷, C. Zhong⁶⁷, X. Zhong⁵⁴, H. Zhou⁴⁵, L.P. Zhou^{1,58}, X. Zhou⁷¹, X.K. Zhou⁵⁸, X.R. Zhou^{66,53}, X.Y. Zhou³⁵, Y.Z. Zhou^{10,f}, J. Zhu³⁹, K. Zhu¹, K.J. Zhu^{1,53,58}, L.X. Zhu⁵⁸, S.H. Zhu⁶⁵, S.Q. Zhu³⁸, T.J. Zhu⁷², W.J. Zhu^{10,f}, Y.C. Zhu^{66,53}, Z.A. Zhu^{1,58}, B.S. Zou¹, J.H. Zou¹, J. Zu^{66,53}

¹ Institute of High Energy Physics, Beijing 100049, People's Republic of China

² Beihang University, Beijing 100191, People's Republic of China

³ Beijing Institute of Petrochemical Technology, Beijing 102617, People's Republic of China

⁴ Bochum Ruhr-University, D-44780 Bochum, Germany

⁵ Carnegie Mellon University, Pittsburgh, Pennsylvania 15213, U.S.A.

⁶ Central China Normal University, Wuhan 430079, People's Republic of China

⁷ Central South University, Changsha 410083, People's Republic of China

⁸ China Center of Advanced Science and Technology, Beijing 100190, People's Republic of China

⁹ COMSATS University Islamabad, Lahore Campus, Defence Road, Off Raiwind Road, 54000 Lahore, Pakistan

¹⁰ Fudan University, Shanghai 200433, People's Republic of China

¹¹ G.I. Budker Institute of Nuclear Physics SB RAS (BINP), Novosibirsk 630090, Russia

- ¹² GSI Helmholtzcentre for Heavy Ion Research GmbH, D-64291 Darmstadt, Germany
- ¹³ Guangxi Normal University, Guilin 541004, People's Republic of China
- ¹⁴ Guangxi University, Nanning 530004, People's Republic of China
- ¹⁵ Hangzhou Normal University, Hangzhou 310036, People's Republic of China
- ¹⁶ Hebei University, Baoding 071002, People's Republic of China
- ¹⁷ Helmholtz Institute Mainz, Staudinger Weg 18, D-55099 Mainz, Germany
- ¹⁸ Henan Normal University, Xinxiang 453007, People's Republic of China
- ¹⁹ Henan University of Science and Technology, Luoyang 471003, People's Republic of China
- ²⁰ Henan University of Technology, Zhengzhou 450001, People's Republic of China
- ²¹ Huangshan College, Huangshan 245000, People's Republic of China
- ²² Hunan Normal University, Changsha 410081, People's Republic of China
- ²³ Hunan University, Changsha 410082, People's Republic of China
- ²⁴ Indian Institute of Technology Madras, Chennai 600036, India
- ²⁵ Indiana University, Bloomington, Indiana 47405, U.S.A.
- ²⁶ INFN Laboratori Nazionali di Frascati, (A)INFN Laboratori Nazionali di Frascati, I-00044, Frascati, Italy; (B)INFN Sezione di Perugia, I-06100, Perugia, Italy; (C)University of Perugia, I-06100, Perugia, Italy
- ²⁷ INFN Sezione di Ferrara, (A)INFN Sezione di Ferrara, I-44122, Ferrara, Italy; (B)University of Ferrara, I-44122, Ferrara, Italy
- ²⁸ Institute of Modern Physics, Lanzhou 730000, People's Republic of China
- ²⁹ Institute of Physics and Technology, Peace Avenue 54B, Ulaanbaatar 13330, Mongolia
- ³⁰ Jilin University, Changchun 130012, People's Republic of China
- ³¹ Johannes Gutenberg University of Mainz, Johann-Joachim-Becher-Weg 45, D-55099 Mainz, Germany
- ³² Joint Institute for Nuclear Research, 141980 Dubna, Moscow region, Russia
- ³³ Justus-Liebig-Universitaet Giessen, II. Physikalisches Institut, Heinrich-Buff-Ring 16, D-35392 Giessen, Germany
- ³⁴ Lanzhou University, Lanzhou 730000, People's Republic of China
- ³⁵ Liaoning Normal University, Dalian 116029, People's Republic of China
- ³⁶ Liaoning University, Shenyang 110036, People's Republic of China
- ³⁷ Nanjing Normal University, Nanjing 210023, People's Republic of China
- ³⁸ Nanjing University, Nanjing 210093, People's Republic of China
- ³⁹ Nankai University, Tianjin 300071, People's Republic of China
- ⁴⁰ National Centre for Nuclear Research, Warsaw 02-093, Poland
- ⁴¹ North China Electric Power University, Beijing 102206, People's Republic of China
- ⁴² Peking University, Beijing 100871, People's Republic of China
- ⁴³ Qufu Normal University, Qufu 273165, People's Republic of China
- ⁴⁴ Shandong Normal University, Jinan 250014, People's Republic of China
- ⁴⁵ Shandong University, Jinan 250100, People's Republic of China
- ⁴⁶ Shanghai Jiao Tong University, Shanghai 200240, People's Republic of China
- ⁴⁷ Shanxi Normal University, Linfen 041004, People's Republic of China
- ⁴⁸ Shanxi University, Taiyuan 030006, People's Republic of China
- ⁴⁹ Sichuan University, Chengdu 610064, People's Republic of China
- ⁵⁰ Soochow University, Suzhou 215006, People's Republic of China
- ⁵¹ South China Normal University, Guangzhou 510006, People's Republic of China
- ⁵² Southeast University, Nanjing 211100, People's Republic of China
- ⁵³ State Key Laboratory of Particle Detection and Electronics, Beijing 100049, Hefei 230026, People's Republic of China
- ⁵⁴ Sun Yat-Sen University, Guangzhou 510275, People's Republic of China
- ⁵⁵ Suranaree University of Technology, University Avenue 111, Nakhon Ratchasima 30000, Thailand
- ⁵⁶ Tsinghua University, Beijing 100084, People's Republic of China
- ⁵⁷ Turkish Accelerator Center Particle Factory Group, (A)Istinye University, 34010, Istanbul, Turkey; (B)Near East University, Nicosia, North Cyprus, Mersin 10, Turkey

- ⁵⁸ *University of Chinese Academy of Sciences, Beijing 100049, People’s Republic of China*
- ⁵⁹ *University of Groningen, NL-9747 AA Groningen, The Netherlands*
- ⁶⁰ *University of Hawaii, Honolulu, Hawaii 96822, U.S.A.*
- ⁶¹ *University of Jinan, Jinan 250022, People’s Republic of China*
- ⁶² *University of Manchester, Oxford Road, Manchester, M13 9PL, United Kingdom*
- ⁶³ *University of Muenster, Wilhelm-Klemm-Strasse 9, 48149 Muenster, Germany*
- ⁶⁴ *University of Oxford, Keble Road, Oxford OX13RH, United Kingdom*
- ⁶⁵ *University of Science and Technology Liaoning, Anshan 114051, People’s Republic of China*
- ⁶⁶ *University of Science and Technology of China, Hefei 230026, People’s Republic of China*
- ⁶⁷ *University of South China, Hengyang 421001, People’s Republic of China*
- ⁶⁸ *University of the Punjab, Lahore-54590, Pakistan*
- ⁶⁹ *University of Turin and INFN, (A)University of Turin, I-10125, Turin, Italy; (B)University of Eastern Piedmont, I-15121, Alessandria, Italy; (C)INFN, I-10125, Turin, Italy*
- ⁷⁰ *Uppsala University, Box 516, SE-75120 Uppsala, Sweden*
- ⁷¹ *Wuhan University, Wuhan 430072, People’s Republic of China*
- ⁷² *Xinyang Normal University, Xinyang 464000, People’s Republic of China*
- ⁷³ *Yunnan University, Kunming 650500, People’s Republic of China*
- ⁷⁴ *Zhejiang University, Hangzhou 310027, People’s Republic of China*
- ⁷⁵ *Zhengzhou University, Zhengzhou 450001, People’s Republic of China*
- ^a *Also at the Moscow Institute of Physics and Technology, Moscow 141700, Russia*
- ^b *Also at the Novosibirsk State University, Novosibirsk, 630090, Russia*
- ^c *Also at the NRC “Kurchatov Institute”, PNPI, 188300, Gatchina, Russia*
- ^d *Also at Goethe University Frankfurt, 60323 Frankfurt am Main, Germany*
- ^e *Also at Key Laboratory for Particle Physics, Astrophysics and Cosmology, Ministry of Education; Shanghai Key Laboratory for Particle Physics and Cosmology; Institute of Nuclear and Particle Physics, Shanghai 200240, People’s Republic of China*
- ^f *Also at Key Laboratory of Nuclear Physics and Ion-beam Application (MOE) and Institute of Modern Physics, Fudan University, Shanghai 200443, People’s Republic of China*
- ^g *Also at State Key Laboratory of Nuclear Physics and Technology, Peking University, Beijing 100871, People’s Republic of China*
- ^h *Also at School of Physics and Electronics, Hunan University, Changsha 410082, China*
- ⁱ *Also at Guangdong Provincial Key Laboratory of Nuclear Science, Institute of Quantum Matter, South China Normal University, Guangzhou 510006, China*
- ^j *Also at Frontiers Science Center for Rare Isotopes, Lanzhou University, Lanzhou 730000, People’s Republic of China*
- ^k *Also at Lanzhou Center for Theoretical Physics, Lanzhou University, Lanzhou 730000, People’s Republic of China*
- ^l *Also at the Department of Mathematical Sciences, IBA, Karachi, Pakistan*